

PSFC/JA-10-66

**Loss Estimate for ITER ECH Transmission Line
Including Multimode Propagation**

Shapiro, M.A., Kowalski, E.J., Sirigiri, J.R., Tax, D.S., Temkin,
R.J., Bigelow, T.S.*, Caughman, J.B.*, Rasmussen, D.A.*

* Oak Ridge National Laboratory, U.S. ITER Project,
Oak Ridge, Tennessee 37831

2010

**Plasma Science and Fusion Center
Massachusetts Institute of Technology
Cambridge MA 02139 USA**

This research was supported by the U.S. Department of Energy, Office of Fusion Energy Sciences (Grant No. DE-FC02-93ER54186), and by the U.S. ITER Project managed by Battelle/Oak Ridge National Laboratory. Reproduction, translation, publication, use and disposal, in whole or in part, by or for the United States government is permitted.

LOSS ESTIMATE FOR ITER ECH TRANSMISSION LINE INCLUDING MULTIMODE PROPAGATION

M. A. Shapiro, E. J. Kowalski, J. R. Sirigiri, D. S. Tax, and R. J. Temkin

MIT Plasma Science and Fusion Center, Cambridge, Massachusetts 02139, USA

T. S. Bigelow, J. B. Caughman, and D. A. Rasmussen

US ITER Project, Oak Ridge National Laboratory, Oak Ridge, Tennessee 37831, USA

Abstract

The ITER ECH Transmission Lines (TLs) are 63.5 mm diameter corrugated waveguides that will each carry 1 MW of power at 170 GHz with a transmission efficiency that should exceed 83%. The losses on the ITER TL have been calculated for four possible cases corresponding to having HE_{11} mode purity at the input of the TL of 100%, 97%, 90% and 80%. The losses due to coupling, Ohmic and mode conversion loss are evaluated in detail using a numerical code and analytical approaches. Estimates of the calorimetric loss on the line show that the output power is reduced by about 5 ± 1 % due to Ohmic loss in each of the four cases. Estimates of the mode conversion loss show that the fraction of output power in the HE_{11} mode is about 3% smaller than the fraction of input power in the HE_{11} mode. High output mode purity therefore can only be achieved with significantly higher input mode purity. Combining both Ohmic and mode conversion loss, for 1 MW of power generated by the gyrotron, the output power in the HE_{11} mode at the end of the ITER TL can be roughly estimated in theory as 920 kW times the fraction of input power in the HE_{11} mode.

I. INTRODUCTION

I.A. ITER ECH/ECCD SYSTEM

Electron-cyclotron heating (ECH) and electron-cyclotron current drive (ECCD) in ITER will be provided by twenty-four 1 MW, 170 GHz gyrotrons^{1,2}. Figure 1 is a schematic of the ECH/ECCD system of ITER³. The transmission line (TL) connects the gyrotron system to the ECH launcher (equatorial launcher and upper launchers)⁴⁻⁶. The ITER requirement for the efficiency of the transmission lines is governed by the specification that a total power of 20 MW should be delivered to the plasma out of the 24 MW generated by the gyrotrons. Therefore, the efficiency of the ECH system including the TLs and ECH launchers should exceed 83%. Since the ECH system contains many complex components and presents a long transmission length, it is a challenge to meet the ITER requirement on transmission losses. The efficiency of transmission lines that carry megawatt power level gyrotron radiation is a topic of intensive present day research⁷⁻¹⁶.

Figure 2 presents a schematic of the TL connecting the gyrotron to the equatorial launcher. The microwave power is transmitted using 63.5 mm diameter corrugated waveguides. Along with the straight waveguide sections and miter bends, the TL contains polarizers (combined with the miter bends), valves, dc breaks, pumping sections, releasers, windows and other components. The transmission lines for the ITER ECH system are still under design and the schematic shown in Fig. 2 should be understood as an example of the configuration. The final configuration may be different.

The HE_{11} mode of a corrugated waveguide is the operating mode of the TL. The TL provides extremely low Ohmic loss of the HE_{11} mode in the straight waveguide sections. Mode conversion losses of the HE_{11} mode occur primarily in the miter bends, gaps and other components. In previous research on ECH TLs, it has been generally assumed that the mode excited at the entrance to the line is a pure HE_{11} mode^{8,17}. However, research shows that gyrotron beams coupled onto the TL often excite high order modes (HOMs) in addition to the fundamental HE_{11} mode. The excitation of HOMs is caused by imperfections in the Gaussian-like beam from the gyrotron (phase errors, incorrect waist size, etc.) as well as coupling errors of the beam into the guide (tilt, offset)¹⁷. The purpose of this paper is to calculate the losses on the ITER ECH TL for realistic cases that include HOM excitation on the transmission line.

This paper presents an estimate of the losses for four cases of power transmission in the ITER ECH transmission line (TL). The four cases represent different levels of the efficiency of excitation of the fundamental HE_{11} mode in coupling of the microwave beam from the gyrotron onto the ECH line.

I.B. REPRESENTATIVE ITER TRANSMISSION LINE COMPONENTS

The design of the ITER transmission line is still ongoing³. For the present calculations, our goal is an understanding of the role of HOMs in the power transmission and the mode conversion on the TL. Therefore, we have used an available, older model of the transmission line, which is described in Table 1. The present results are illustrative of the calculation methods and can be easily refined as the TL design changes. Changes in

the design of the TL will change the numerical results but should not change the conclusions of this study.

The parameters in Table 1 were taken from the 2007 ITER design for the TL to the equatorial ECH launcher. Nine waveguide (WG) sections and eight miter bends (MBs) are used in this TL (Table 1). The first two miter bends serve as polarizers. In this calculation, we include the possibility that the miter bend mirrors have small fabrication errors, amounting to a tilt of ± 0.025 deg. The tilt is entered by specifying the specific values shown in Table 1. Introduction of this tilt will result in some mode conversion. A 20-micron bulge of the miter bend mirrors due to heating was calculated, but its effect on the performance of the miter bend was found to be insignificant.

II. LINEARLY POLARIZED LP_{mn} MODES OF CORRUGATED WAVEGUIDE

The present work differs from previous approaches in the exclusive use of linearly polarized modes (LP_{mn} , m is the azimuthal index, and n is the radial index) to describe the modes excited on the TL. The beam from the gyrotron is usually close to 100% linearly polarized. This microwave beam will excite the linearly polarized modes (LP_{mn} modes) of the waveguide. The LP_{mn} modes of corrugated metallic waveguide were first discussed in Ref. 19, where it is shown that the lowest modes, the LP_{11} modes could be constructed from the usual eigenmodes of the corrugated waveguide. The set of LP_{mn} modes may be used in a corrugated waveguide if the corrugation depth is a quarter of a wavelength.

Linearly polarized modes LP_{mn} can be constructed as a superposition of the HE, EH, TE, and TM modes of a corrugated waveguide. The transverse electric field in the LP_{mn} modes can be expressed as follows (for polarization along the y-axis):

$$\vec{E}_{mn}^{\perp} = \frac{X_n}{a} J_m \left(X_n \frac{r}{a} \right) \cos(m\phi) \hat{y} \quad (\text{LP}_{mn} \text{ even mode}) \quad (1)$$

$$\vec{E}_{mn}^{\perp} = \frac{X_n}{a} J_m \left(X_n \frac{r}{a} \right) \sin(m\phi) \hat{y} \quad (\text{LP}_{mn} \text{ odd mode})$$

where (r, ϕ) are the polar coordinates, a is the waveguide radius, X_n is the n -th zero of the Bessel function J_m . Note that the LP_{0n} modes are the same as the HE_{1n} modes, and we use the latter notation in this paper. If some fraction of the incident power is in the transverse polarization, that power may transit the TL but will not be efficient for ECH or ECCD. Therefore, the power in the wrong polarization can just be considered lost power and will not be included here.

III. TRANSMISSION LINE LOSS: OVERVIEW

The loss on the ITER TL consists of three components:

- 1.) Coupling Loss
- 2.) Calorimetric Loss
- 3.) Mode Conversion Loss

The first component of loss is the coupling loss. It occurs when the microwave beam from the gyrotron couples to the HE_{11} mode of the TL with less than 100% efficiency. The second component of loss is calorimetric loss. This loss occurs when modes are absorbed along the TL by ohmic loss. The third component of loss is mode conversion loss. Mode conversion at miter bends, gaps and other components results in power exiting the TL in modes other than the desired HE_{11} mode. These different loss mechanisms are taken into account in the loss calculations presented in this paper.

III.A. Coupling of Power into the ITER Transmission Line

The output beam from the gyrotron is assumed to be a slightly imperfect Gaussian beam (GB) containing 1 MW of power. We allow some variation in waist size and beam tilt. Four examples of mode excitation of the corrugated waveguide by a GB are presented in Table 2. Each case represents different GB coupling parameters. These coupling examples differ by the HE_{11} mode power excited in the waveguide. The percentage of the HE_{11} mode varies when the GB parameters change (the beam waist size, tilt angle, or beam offset). The cases labeled 2, 3 and 4 are only representative values. For example, it is possible to construct another version of case 3, with 90% efficiency of excitation of the HE_{11} mode, using different values of the GB waist, tilt, etc.

The coupling of a Gaussian Beam into a corrugated waveguide has been calculated in detail by Ohkubo et al.¹⁸ We have used the same approach and written a code to calculate the coupling of the field of the Gaussian Beam onto the LP_{mn} modes of

the corrugated waveguide. We also take into account a small truncation loss that arises because a small portion of the Gaussian Beam is outside of the 63.5 mm waveguide aperture. This amounts to about a 1 % reduction in power coupled onto the TL for cases 2, 3 and 4 of Table 2. Since we have assumed that the Gaussian Beam from the gyrotron has 1 MW of power, this truncation loss will be treated as equivalent to ohmic loss in the calculations that are presented in this paper.

III.B. Ohmic Loss

Ohmic loss occurs in transmission through the straight sections and in reflection from mirrors or polarizers at the miter bends. A detailed calculation of the Ohmic loss in the straight sections has been given recently by Doane⁹ and we have used his estimate in Table 3. The Ohmic loss at a miter bend is given by:

$$Loss = 1.2 * 4 \frac{R_s}{Z_0} \begin{bmatrix} \cos \alpha \\ 1 / \cos \alpha \end{bmatrix} \begin{matrix} \text{H-Plane} \\ \text{E-Plane} \end{matrix}$$

where R_s is the surface resistance, $Z_0=377 \Omega$ is the impedance of free space, α is the incidence angle.

For room temperature copper, the loss is 0.10% for an H-plane bend and 0.19% for an E-plane bend. For convenience, we use a weighted average value of 0.14% for each bend in the TL. The loss at polarizers is estimated as double that at a conventional bend. The Ohmic loss parameters for the waveguide straight sections and miter bend mirrors are listed in Table 3.

III.C. Simulation of Loss due to Diffraction in a Miter Bend

Diffraction at a miter bend leads to the excitation of higher order modes at the output port of the bend. This loss has been previously estimated by Doane and Moeller¹⁷. However, their results were obtained exclusively for the HE_{11} and TE_{01} modes. We have extended that theory to estimate the loss for higher order LP_{mn} modes. However, we have found it to be more convenient to develop a completely new code to simulate mode conversion and losses in a miter bend and have used our code in analyzing the ITER ECH Transmission Line (TL).

Our propagation code simulates mode conversion in miter bends for an arbitrary input mode mixture. The ability to treat a mixture of modes is important because the gyrotron output radiation excites a mixture of modes in the corrugated waveguide, not a pure HE_{11} mode. The code calculates the mode mixture at the exit port of a miter bend for any input of a sum of LP_{mn} modes of arbitrary relative phase. Power converted into HOMs is tracked in the calculation for the first 110 LP_{mn} modes of the waveguide, which is sufficient for the accuracy needed in this calculation.

The code is based on a Fast Fourier Transform (FFT) calculation advancing the fields through the miter bends. Straight sections are calculated analytically. The FFT code was developed to simulate field propagation in the equivalent circuit of a miter bend (Fig. 3, right). The method of the FFT calculation is based on the calculation of the field in a square box whose dimensions are larger than the size of the circular guide. Figure 4

shows the sequence of cross-sections used in the FFT simulation. At the beginning of the calculation, the field of the LP_{mn} mode is confined to the 63.5 mm circular aperture and is zero outside the circular aperture. The code calculates the field progressively along the direction of the waveguide. The outer square aperture remains constant but the cross section of the inner waveguide varies from a circular to a rectangular aperture and back (Fig. 4).

The field is represented by the superposition of modes of the square area with sides L in Cartesian coordinates:

$$A(x, y) \exp(j\varphi(x, y)) = \sum D_{pq} \sin\left(\frac{p\pi x}{L}\right) \sin\left(\frac{q\pi y}{L}\right) \quad (2)$$

where $A(x, y)$ is the linearly polarized field amplitude and $\varphi(x, y)$ is the phase. The coefficients D_{pq} are determined by applying a Fast Fourier Transform (FFT).

As previously mentioned, the fields within the metal region of the cross-section must be identically zero. This will be the case for each cross-section; however we note that the fields will be allowed to have a non-zero magnitude within the slots on the sides. Let us now explore how the fields are propagated at each step. The propagation distance for each step will be $\Delta z = 2a/N$, with N being the total number of steps to cross the gap region. Recall that the fields are represented as a series of modes of the square cavity, shown in Eq. (2). The propagation constant for each mode is therefore defined as:

$$k_{z,pq} = \sqrt{k^2 - \left(\frac{p\pi}{L}\right)^2 - \left(\frac{q\pi}{L}\right)^2} \quad (3)$$

where $k = \omega/c$. We now propagate these fields by one step:

$$A \exp(j\varphi)_{(1)} = \sum D_{pq} \sin\left(\frac{p\pi x}{L}\right) \sin\left(\frac{q\pi y}{L}\right) \exp(jk_{z,pq} \Delta z) \quad (4)$$

The new field amplitude should be zeroed out if it falls into the shaded region (Fig. 4) at the new cross-section. To account for this, we take the inverse FFT of the series of modes, returning to the domain of an array of field amplitudes and phases. We define a new amplitude $\tilde{A} \exp(j\varphi)_{(1)}$ that has been truncated by the shaded region. The fractional loss due to truncation from propagating across the first step is:

$$T_1 = \frac{\int A_{(1)}^2 dx dy - \int \tilde{A}_{(1)}^2 dx dy}{\int A_{(1)}^2 dx dy} \quad (5)$$

We then take $\tilde{A} \exp(j\varphi)_{(1)}$ and as was the case with our initial function, we represent it as a series of modes of the square box by taking the FFT. This function is then propagated to the next cross-section where we take the inverse FFT, truncate the fields and calculate the loss once again. This process is repeated step-by-step until the whole gap region has been traversed and we obtain a final function $\tilde{A} \exp(j\varphi)_{(N)}$. This final function is then decomposed into a series of LP_{mn} modes of the corrugated waveguide. For the calculations presented here, the number of steps, N , is 200 and the

size of the calculation region, the square of side L , is $L=127$ mm. Increasing N or L does not significantly change the results of the calculation.

The final result of each simulation can be broken down into three components: HE_{11} mode transmission; output power appearing at the output port in higher order modes; and a truncation loss of power that does not reach the output port, that is defined as

$$T_{GAP}(dB) = \sum_{n=1}^N T_n(dB) \quad (6)$$

where the fractional loss Eq. (5) is converted to dB.

To validate the FFT code, we have calculated the loss in an axially symmetrical gap of length $2a$ in a corrugated waveguide of diameter $2a$ for the HE_{11} mode using this new approach and compared the results with the Doane and Moeller theory¹⁷. The agreement for two examples, shown in Table 4, is excellent.

The diffraction in the non-symmetrical gap shown in Fig. 3 (right) results in two distinct loss mechanisms:

- (1) Mode conversion into higher order modes (HOMs) in the receiving port. The HOMs that are excited in the receiving port are often capable of propagating down the transmission line. They do not induce large Ohmic loss near the miter bend.
- (2) Radiation from the input port that misses the output port. In a closed miter bend geometry (Fig. 3, left), the radiation that misses the receiving port excites very high order modes (VHOMs). These VHOMs are close to cutoff in highly overmoded waveguide and are dissipated through Ohmic losses in the waveguide near the miter bend.

Table 5 contains the results of miter bend diffractive loss calculations for two miter bends: the ITER 170 GHz miter bend and the General Atomics (GA) 110 GHz miter bend. The results shown for the theory¹⁷ are obtained from an axially symmetrical gap calculation. Doane and Moeller argue that the loss in a miter bend is one half the loss in a gap of length $2a$, since the diffraction effect is the same in both cases but in the miter bend one half of the wall is covered by waveguide (see Ref. 17). The entries for the Doane calculation in Table 5 are obtained by taking one half of the loss from the gap calculation shown in Table 4. The FFT calculations of the miter bend loss (Table 5) agree reasonably well with Ref. 17. Table 5 indicates that the ITER miter bend, more oversized than the GA miter bend, can be more accurately estimated by the Doane and Moeller theory. The percentage of loss due to mode conversion into VHOMs is also given in Table 5 from the FFT code. The VHOM power is estimated from the power that does not reach the output port. This code may also be used when the field at the input port is a mixture of waveguide LP_{mn} modes. In that case, if two modes are present at the input port with the same symmetry (the same m value, but different n values), the modes will interfere at the output port. The resulting mode conversion in the miter bend will be a function of the relative phase of the two modes at the input port²⁰. Our code naturally incorporates this effect. Since the relative phase at subsequent miter bends will depend on the exact distance separating the bends, the effect depends strongly on the exact design of the ITER TL. When averaged over a large number of miter bends, it is hoped that the relative phase will tend to be somewhat random, thus minimizing this effect.

In addition to the loss caused by diffraction, there will also be miter bend loss caused by Ohmic loss on reflection from the miter bend mirror; diffraction loss if the

miter bend mirror is tilted away from exactly 90 degrees, etc. These additional losses are taken into account in the calculation of total loss in the ITER TL.

IV. Loss on the ITER Transmission Line: Results for a Pure LP_{mn} mode

We first consider the transmission of individual, pure LP_{mn} modes on the ITER ECH transmission line. The ITER TL parameters used in these calculations are given in Table 1. Figure 5 shows loss calculation results for the lowest order modes propagating in the ITER corrugated waveguide TL. The calculated losses include:

(1) Miter bend mode conversion loss into very high order modes (VHOMs). These modes are forward and backward modes (see Ref. 17). They are trapped in the waveguide near the miter bend and dissipated through Ohmic loss.

(2) Ohmic loss (Table 3) in the straight waveguide sections.

(3) Ohmic loss in the miter bend mirror (Table 3).

(4) Loss due to mode conversion to other modes, which are High Order Modes (HOMs) that transit the TL to the output port.

The loss components (1), (2), and (3) combine to create calorimetric loss, which is the power loss port-to-port. In addition to that, there is loss (4) associated with output modes other than the pure input mode.

The loss in Figure 5 for the pure HE_{11} mode is similar to the value obtained in previous analysis of the ITER TL loss ⁹. We have calculated the loss for a series of pure LP_{mn} modes; only the lowest order modes are shown in Fig. 5.

Figure 6 shows the output mode content for a pure HE_{11} mode input. As shown in Fig. 5, for the HE_{11} mode, the “Loss due to power in other modes” is 3.4%. Figure 6 illustrates how this 3.4% of power is distributed among the HOMs. Figure 6 shows that the next mode up from the HE_{11} mode, the LP_{11} mode (odd and even), is the most likely mode to be excited due to mode conversion on the ITER TL.

V. Loss on the ITER Transmission Line: Results for a Mixture of LP_{mn} modes

In the previous section, we calculated the loss on the ITER TLs for pure LP_{mn} modes. In this section, we consider mixtures of modes. The mixtures considered are those previously labeled Cases 2, 3 and 4. However, for completeness and comparison, we will also include Case 1, which is a pure mode case. The loss on the ITER TL has three components: coupling loss; mode conversion loss; and ohmic or calorimetric loss. Case 1 is a pure HE_{11} mode; Case 2 is a mixture of modes with 3% HOM content; Case 3 has 10% HOM content and Case 4 has 20% HOM content. Cases 1 and 2 are ideal examples, while Cases 3 and 4 may be more realistic examples.

Mode Conversion Loss for a Mixture of LP_{mn} modes

The results for Case 1 were reported in the previous section, which treated the case of pure modes. The results for mode conversion for Case 2 are in Fig. 7; for Case 3 in Fig. 8 and for Case 4 in Fig. 9. Figures 7, 8 and 9 show the mode mixtures on the TL at two locations: at the input port and at the output port. For each mode, the power is reported as the percentage of power in the given LP_{mn} mode divided by the total power in all modes. Figure 7 shows the result for Case 2 with 3% HOMs at the input. These results show that there is a modest increase of HOMs at the output port, particularly the LP_{11} modes (even and odd). Figures 8 and 9 show similar behavior for the cases with larger HOM content at the input port. For clarity, we show in Fig. 10 the fraction of power in the HE_{11} mode at the output port for each of the four Cases. The information in Fig. 10 is also evident in Figs. 6-9, but is hard to read in those figures.

Calculation of Calorimetric Power Loss in the TL

Figure 11 shows the calorimetric loss for the four Cases. There are four sources of calorimetric loss:

- 1) Truncation loss. This loss occurs because the nearly Gaussian beam at the TL input port has a small fraction of power, about 1% as seen in Fig. 11, which is outside of the 63.5 mm waveguide diameter aperture. In the ideal case, Case 1 of a pure HE_{11} mode, this loss is zero.

- 2) MB Loss, VHOMs. This loss is due to the excitation of very high order modes (VHOMs) at a miter bend.
- 3) Ohmic loss in straight sections.
- 4) Ohmic loss upon reflection at miter bend and polarizer mirrors.

Calorimetric loss is distinguished from mode conversion loss. In miter bends, significant mode conversion loss occurs into lower order modes of the waveguide. These modes can transit the entire ITER ECH TL. This can be seen from the results shown for individual modes in Fig. 7. For example, the HE_{13} mode has 30% loss for the entire line, so that the majority of power converted into this mode at miter bends would appear at the output port. Mode conversion to VHOMs that are near cutoff results in modes that do not transit the line and thus produce Ohmic or calorimetric loss. The code used for these calculations tracks the lowest 110 LP_{mn} modes of the TL and thus accounts with high accuracy the ohmic loss due to higher order modes. Since the HE_{11} mode is the majority of power in each case, the calorimetric loss is similar for all of the cases in Fig. 11.

VI. Summary of HE_{11} mode Output Power for the Four Cases

The results of the calculations are summarized here. We are interested in the output power that is in the HE_{11} mode in each of the four cases, since only the power in the HE_{11} mode will be properly launched into the ITER plasma. The power at the output port that is not in the HE_{11} mode is shown in Fig. 12. The lost power has three main components:

- 1) Coupling Loss, which is power that did not couple into the TL at the input port.
- 2) Ohmic (calorimetric) loss due to VHOM modes at miter bends, straight section ohmic loss and mirror ohmic loss.
- 3) Mode conversion loss due to mode conversion at the miter bends, and also due to waveguide sag, and tilt and offset at waveguide junctions.

We also include mode conversion loss at the input port in calculating the total mode conversion loss. The loss due to sagging, tilt, and offset of straight waveguide sections was estimated by Doane⁹ as 0.075 dB (or 1.7% fractional loss). This loss was excluded from Fig. 10 to obtain a clearer result, but must be included in Fig. 12 for the total loss estimate. Figure 11 shows the calorimetric loss. Figure 12 shows the HE₁₁ mode power loss for the four cases.

The final result of the calculation is also listed in Table 6, which shows the losses for a 1 MW, 170 GHz gyrotron beam on the ITER ECH TL for each case. For the results presented in Table 6, the definition of the parameters is given by:

P_{in} (kW) = Power injected into TL from the incident 1 MW gyrotron beam

$P_{in HE_{11}}$ (kW) = Power at the TL entrance port in the HE₁₁ mode

P_{out} (kW) = Total power at the TL exit

$P_{out HE_{11}}$ (kW) = Power at the TL exit in the HE₁₁ mode

Calorimetric Power Loss = $1 - P_{out}$ (kW)/1000

HE₁₁ Mode Loss = $1 - P_{out HE_{11}}$ (kW)/1000

$$\text{Output HE}_{11} \text{ Mode Content} = P_{\text{out HE}_{11}}/P_{\text{out}}$$

We may also show the final results in graphical form, as is done in Fig. 13. We see from Table 6 and Fig. 13 that for 1 MW of power generated by the gyrotron, the output power in the HE₁₁ mode can be roughly estimated as 920 kW times the fraction of input power in the HE₁₁ mode. This estimate can be shown from Fig. 13 to be correct to within 1% error for input power fractions of 80 to 100%. A 97% HE₁₁ mode purity input is required for a 94% mode purity output; this is a very stringent requirement.

VII. CONCLUSIONS

The losses on the ITER ECH Transmission Line have been calculated for four possible cases corresponding to having HE₁₁ mode purity at the input of the TL of 100%, 97%, 90% and 80%. The losses due to coupling, Ohmic and mode conversion loss are evaluated in detail using a numerical code and analytical approaches. Estimates of the calorimetric loss on the line show that the output power is reduced by about 6 ± 1 % due to Ohmic loss in each of the four cases. Estimates of the mode conversion loss show that the fraction of output power in the HE₁₁ mode is about 3% smaller than the fraction of input power in the HE₁₁ mode. High output mode purity therefore can only be achieved with significantly higher input mode purity. Combining both Ohmic and mode conversion loss, for 1 MW of power generated by the gyrotron, the output power in the HE₁₁ mode at the end of the ITER TL can be roughly estimated as 920 kW times the fraction of input power in the HE₁₁ mode.

The loss calculated in this paper is only intended as a representative calculation. Since the design of the ITER TL is not yet fixed, the results may be different for the final TL. However, it is hoped that the present calculation can provide guidance for the expected TL performance under ideal conditions. The present calculations are for an ideal system. A real system will have higher loss than the value calculated here. In a real TL used over a period of time, losses may also increase due to displacement of parts.

Acknowledgments

The authors would like to thank John Doane and Robert Olstad of General Atomics and Mark Henderson of the ITER Organization for helpful discussions.

This research was supported by the US DOE Office of Fusion Energy Sciences and by the US ITER Project managed by Battelle/ORNL.

REFERENCES

1. T. IMAI, N. KOBAYASHI, R. TEMKIN, M. THUMM, M. Q. TRAN and V. ALIKAEV, "ITER R&D: Auxiliary systems: Electron cyclotron heating and current drive system," Fusion Eng. Design, Vol. 55, p. 281 (2001).
2. ITER Detailed Description Document – 5.2 Electron Cyclotron Heating and Current Drive System, G 52 DDD 5 01-05-29, ITER Organization, 2001.
3. M.A. HENDERSON, B. BECKETT, C. DARBOS, N. KOBAYASHI, G. SAIBENE, F. ALBAJAR, T. BONICELLI, S. ALBERTI, R. CHAVAN, D. FASEL, T. P. GOODMAN, I. Gr. PAGONAKIS, O. SAUTER, S. CIRANT, D. FARINA, G. RAMPONI, R. HEIDINGER, B. PIOSZYK, M. THUMM, S.L. RAO, K. KAJIWARA, K. SAKAMOTO, K. TAKAHASHI, G. DENISOV, T. BIGELOW, D. RASMUSSEN, "A Revised ITER EC System Baseline Design Proposal," Proceedings of the Fifteenth Joint Workshop on Electron Cyclotron Emission and Electron Cyclotron Resonance Heating, EC15, J. Lohr (editor), World Scientific, pp. 458-464 (2009).
4. CIRANT, S., "Overview of electron cyclotron heating and electron cyclotron current drive launcher development in magnetic fusion devices," Fusion Science and Technology, v 53, n 1, 12-38, (2008).

5. HENDERSON, M.A.; CHAVAN, R.; BERTTZZOLO, R.; CAMPBELL, D.; DURON, J.; DOLIZY, F.; HEIDINGER, R.; LANDIS, J.-D.; SAIBENE, G.; SANCHEZ, F.; SERIKOV, A.; SHIDARA, H.; SPAEH, P., "Critical Design Issues of the ITER ECH Front Steering Upper Launcher," *Fusion Science and Technology*, v 53, n 1, 139-58, Jan. 2008.
6. HENDERSON, M.A.; SAIBENE, G., "Critical interface issues associated with the ITER EC system," *Nuclear Fusion*, v 48, n 5, p 054017 (15 pp.), May 2008.
7. OLSTAD, R.A.; DOANE, J.L.; MOELLER, C.P. "ECH MW-level CW transmission line components suitable for ITER," *Fusion Engineering and Design*, v 74, n 1-4, p 331-5, Nov. 2005.
8. J. L. DOANE and R. A. OLSTAD, "Transmission Line Technology for Electron Cyclotron Heating," *Fusion Sci. Technol.*, Vol. 53, p.39 (2008).
9. J. L. DOANE, "Design of Circular Corrugated Waveguide to Transmit Millimeter Waves at ITER," *Fusion Sci. Tech.*, Vol. 53, p. 159 (2008).
10. KAJIWARA, K.; TAKAHASHI, K.; KOBAYASHI, N.; KASUGAI, A.; KOBAYASHI, T.; SAKAMOTO, K., "Development of the transmission line and the launcher for the ITER ECH system," 2007 Joint 32nd International Conference on

Infrared and Millimeter Waves and the 15th International Conference on Terahertz Electronics (IRMMW-THz), p 793-4, 2008.

11. HAN, S.T.; COMFOLTEY, E.N.; SHAPIRO, M.A.; SIRIGIRI, J.R.; TAX, D.S.; TEMKIN, R.J.; WOSKOV, P.P.; RASMUSSEN, D.A., “Low-power testing of losses in millimeter-wave transmission lines for high-power applications,” Intl. Journal of Infrared and Millimeter Waves, Vol. 29, No. 11, p 1011-1018 (2008).

12. S. PARK, J. JEONG, W. NAMKUNG, M.-H. CHO, Y. S. BAE, W.-S. HAN, H.-L. YANG, “Commissioning of KSTAR 84-GHz ECH Transmission System,” Fusion Science and Technology, Vol. 55, Pages 56-63. (2009).

13. V. ERCKMANN; W. KASPAREK; G. GANTENBEIN; F. HOLLMANN; L. JONITZ; F. NOKE; F. PURPS; M. WEISSGERBER; “ECRH for W7-X: Transmission Losses of High-Power 140-GHz Wave Beams,” Fusion Sci. Tech., Vol. 55 pp.16-22 (2009).

14. M. CENGHER, J. LOHR, I.A. GORELOV, W.H. GROSNICKLE, D. PONCE, P. JOHNSON, “Measurements of the ECH Power and of the Transmission Line Losses on DIII-D,” Proceedings of the Fifteenth Joint Workshop on Electron Cyclotron Emission and Electron Cyclotron Resonance Heating, EC15, J. Lohr (editor), World Scientific, pp. 483-489 (2009).

15. R.A. OLISTAD, R.W. CALLIS, J.L. DOANE, H.J. GRUNLOH, C.P. MOELLER, “Progress on Design and Testing of Corrugated Waveguide Components Suitable for ITER ECH and CD Transmission Lines,” Proceedings of the Fifteenth Joint Workshop on Electron Cyclotron Emission and Electron Cyclotron Resonance Heating, EC15, J. Lohr (editor), World Scientific, pp. 542-547 (2009).

16. R.W. CALLIS, J.L. DOANE, H.J. GRUNLOH, K. KAJIWARA, A. KASUGAI, C.P. MOELLER, Y. ODA, R.A. OLISTAD, K. SAKAMOTO, K. TAKAHASHI, “Design and testing of ITER ECH & CD transmission line components,” Fusion Engineering and Design, Vol. 84, pp. 526–529 (2009).

17. J. L. DOANE and C. P. MOELLER, “HE₁₁ Bends and Gaps in a Circular Corrugated Waveguide,” Int. Journ. of Electronics, Vol. 77, p. 489 (1994).

18. K. OHKUBO, S. KUBO, H. IDEI, M. SATO, T. SHIMOZUMA, and Y. TAKITA, “Coupling of tilting Gaussian beam with hybrid mode in the corrugated waveguide,” Intl. Journal of Infrared and Millimeter Waves, Vol. 18, No. 1, p 23-41, (1997).

19. CLARRICOATS, P.J.B.; ELLIOT, R.D., “Multimode corrugated waveguide feed for monopulse radar,” IEE Proceedings H (Microwaves, Optics and Antennas), Vol. 128, n 2, p 102-10, (1981).

20. TAX, D.S.; COMFOLTEY, E.N.; HAN, S.-T.; SHAPIRO, M.A.; SIRIGIRI, J.R.; TEMKIN, R.J.; WOSKOV, P.P., “Mode conversion losses in ITER transmission lines,”

Proceedings of the 33rd International Conference on Infrared, Millimeter and Terahertz
Waves (IRMMW-THz 2008), 2 pp., 2008.

Table 1. ITER Waveguide (WG) and Miter Bend (MB) parameters

WG section/MB #	WG Length (m)	MB mirror X/Y-plane tilt (deg.)	Polarizer
1	1.2	0.025 / -0.025	Yes
2	22	-0.025 / 0.025	Yes
3	40	0.025 / -0.025	No
4	9.1	0.025 / -0.025	No
5	8	-0.025 / 0.025	No
6	11	-0.025 / 0.025	No
7	20	0.025 / -0.025	No
8	2.9	-0.025 / 0.025	No
9	8.8		

Table 2. Examples of Coupling of a Gaussian Beam (GB) onto the Transmission Line

Coupling Example	Case	GB waist in Y/X-direction W0 (y/x) (cm)	GB tilt in Y/X-direction (deg.)	GB offset in Y/X-direction (cm)	Fraction of Input Power in the HE ₁₁ mode
100% HE ₁₁	1	2.03 / 2.03	0 / 0	0 / 0	100%
97% HE ₁₁	2	2.08 / 1.98	0.07 / 0.07	0.07 / 0.07	97%
90% HE ₁₁	3	2.18 / 1.98	0.3 / 0.3	0.1 / 0.2	90%
80% HE ₁₁	4	2.18 / 1.98	0.45 / 0.5	0.1 / 0.2	80%

Table 3. Ohmic Loss Parameters

Straight sec. HE ₁₁ mode Ohmic loss (amplitude decrement, Np/m)	0.18E-4
MB Mirror Ohmic Loss (fractional)	0.14E-2 (w/o Polarizer) / 0.28E-2 (w/ Polarizer)

Table 4: Calculation of Loss in a Waveguide Gap of Length $2a$

WG diameter ($2a$) and Frequency	Gap Loss (Ref. 17)	Gap Loss (this calculation)
63.5 mm dia. / 170 GHz	0.022 dB	0.022 dB
31.75 mm dia. / 110 GHz	0.120 dB	0.125 dB

Table 5: Miter Bend (MB) Loss

MB Parameters	MB Loss (Ref. 17)	MB Loss (this calc.)	Percentage of Loss to VHOMs (this calc.)
170 GHz/ 63.5 mm dia.	0.011 dB	0.013 dB	47%
110 GHz/ 31.75 mm dia.	0.060 dB	0.085 dB	56%

Table 6. Input and output power levels for 1 MW gyrotron beam.

Case	P_{in} (kW)	P_{in} HE_{11} (kW)	P_{in} HE_{11}/P_{in}	P_{out} (kW)	P_{out} HE_{11} (kW)	P_{out} HE_{11}/P_{out}
1: 100% HE_{11}	1000	1000	1.00	969	920	0.95
2: 97% HE_{11}	991	965	0.97	955	895	0.94
3: 90% HE_{11}	987	886	0.90	950	817	0.86
4: 80% HE_{11}	987	794	0.80	949	732	0.77

FIGURE CAPTIONS

Figure 1. Schematic of ITER ECH System (Ref. 3).

Figure 2. Schematic of the ITER Transmission Line to the Equatorial Launcher.

Figure 3. Miter Bend (left) and its equivalent circuit (right).

Figure 4. Illustration of waveguide cross-section variation used for FFT simulation of the miter bend equivalent circuit (Fig. 3).

Figure 5. Loss (%) in the ITER TL for pure mode input. Partitions: (1) Loss in the miter bends due to excitation of very high order modes which add to Ohmic loss; (2) Ohmic loss in straight sections; (3) Ohmic loss in the miter bend mirrors; (4) Loss due to mode conversion to power in other modes.

Figure 6. Percentage of power in the output for the pure HE_{11} mode input in the ITER TL.

Figure 7. Percentage of modal power in the input and output for the Gaussian beam input that is 97% of HE_{11} mode.

Figure 8. Percentage of modal power in the input and output for the Gaussian beam input that is 90% of HE_{11} mode.

Figure 9. Percentage of modal power in the input and output for the Gaussian beam input that is 80% of HE_{11} mode.

Figure 10. Output HE_{11} mode content: (a) pure HE_{11} mode input; (b)-(d) GB input that is (b) 97% HE_{11} , (c) 90% HE_{11} , (d) 80% HE_{11} .

Figure 11. Calorimetric loss (%) in the ITER TL for (a) pure HE_{11} mode input, (b) Gaussian beam input that is 97% HE_{11} mode, (c) GB that is 90% HE_{11} , (d) GB that is 80% HE_{11} . Partitions: (1) Coupling losses; (2) Losses in the miter bends due to excitation of very high order modes which add to Ohmic losses; (3) Ohmic losses in straight sections; (4) Ohmic losses in the miter bend mirrors.

Figure 12. HE_{11} mode Power Loss (%) in the ITER TL for (a) pure HE_{11} mode input, (b) Gaussian beam input that is 97% HE_{11} mode, (c) GB that is 90% HE_{11} , (d) GB that is 80% HE_{11} . Partitions: (1) Coupling losses; (2) Losses in the miter bends due to excitation of very high order modes which add to Ohmic losses; (3) Ohmic losses in straight sections; (4) Ohmic losses in the miter bend mirrors; (5) HE_{11} mode conversion loss due to sag in waveguide sections and tilt and offset of waveguide section junctions; (6) Losses due to higher order modes in the output beam.

Figure 13. Output power in the HE_{11} mode versus Percentage of HE_{11} in the input.

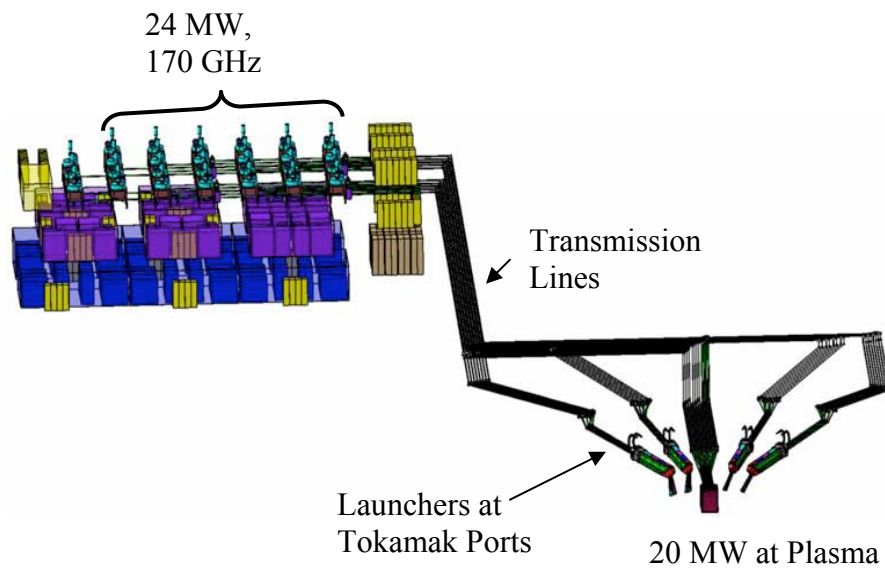


Figure 1. Schematic of ITER ECH System (Ref. 3).

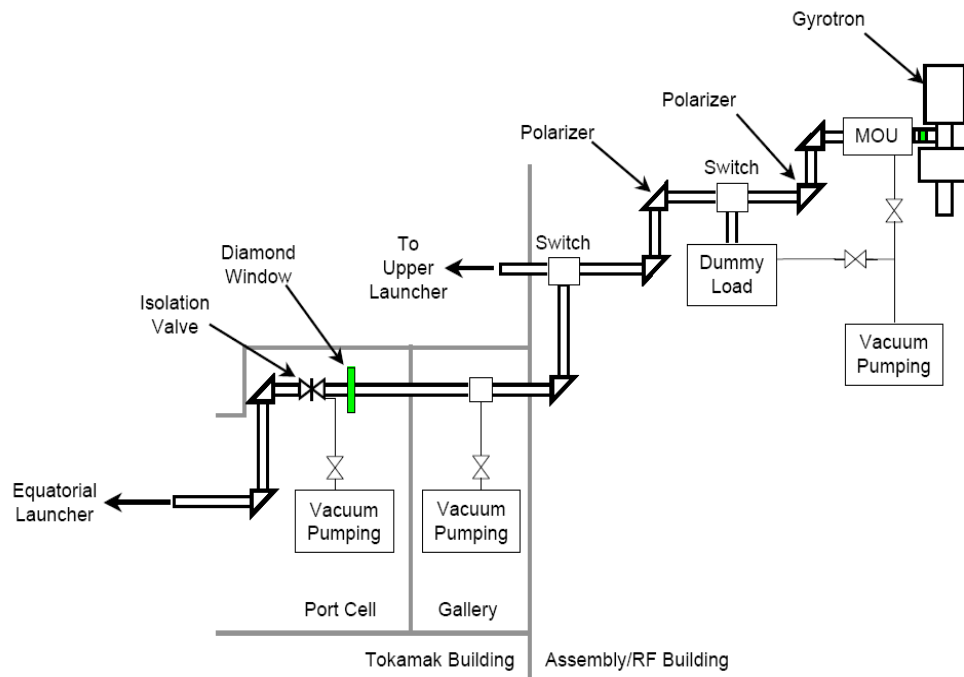


Figure 2. Schematic of the ITER Transmission Line to the Equatorial Launcher.

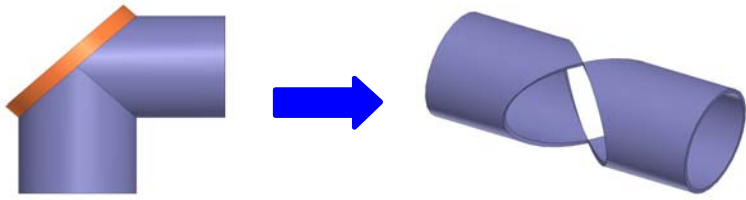


Figure 3. Miter Bend (left) and its equivalent circuit (right).

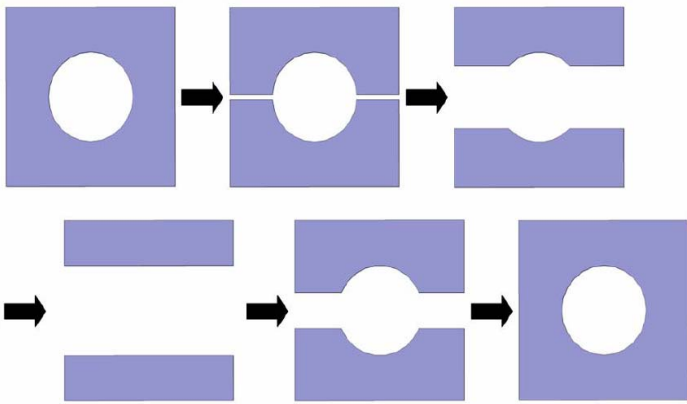


Figure 4. Illustration of waveguide cross-section variation used for FFT simulation of the miter bend equivalent circuit (Fig. 3).

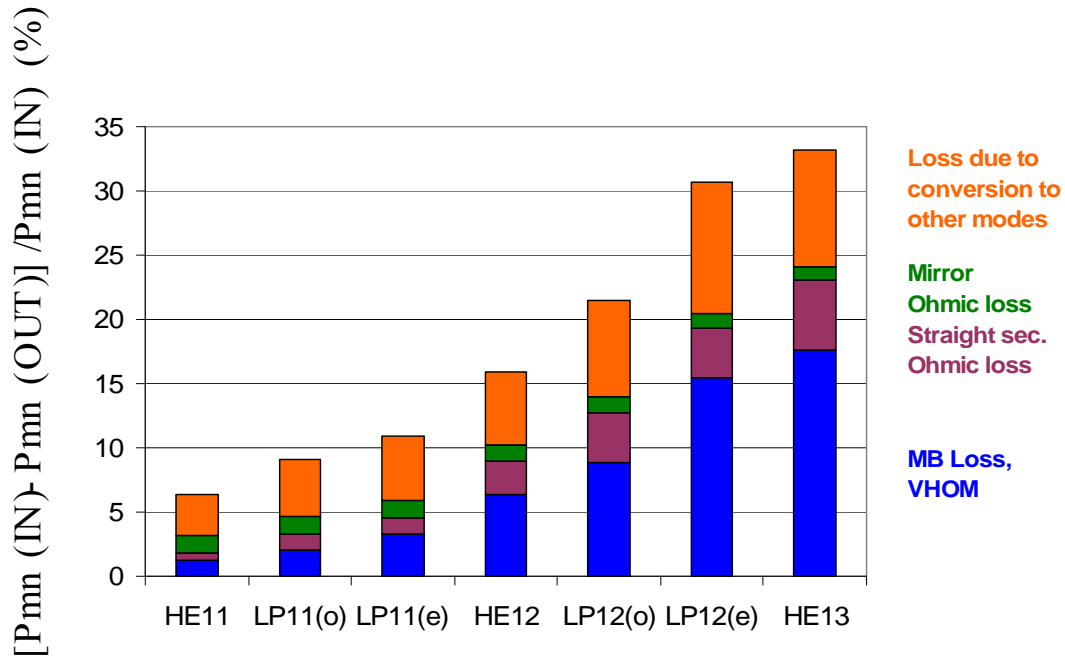


Figure 5. Loss (%) in the ITER TL for pure mode input. Partitions: (1) Loss in the miter bends due to excitation of very high order modes which add to Ohmic loss; (2) Ohmic loss in straight sections; (3) Ohmic loss in the miter bend mirrors; (4) Loss due to mode conversion to power in other modes.

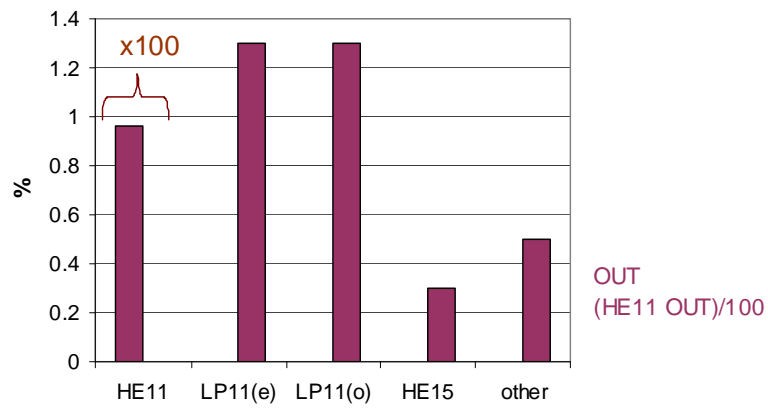


Figure 6. Percentage of power in the output for the pure HE₁₁ mode input in the ITER TL.

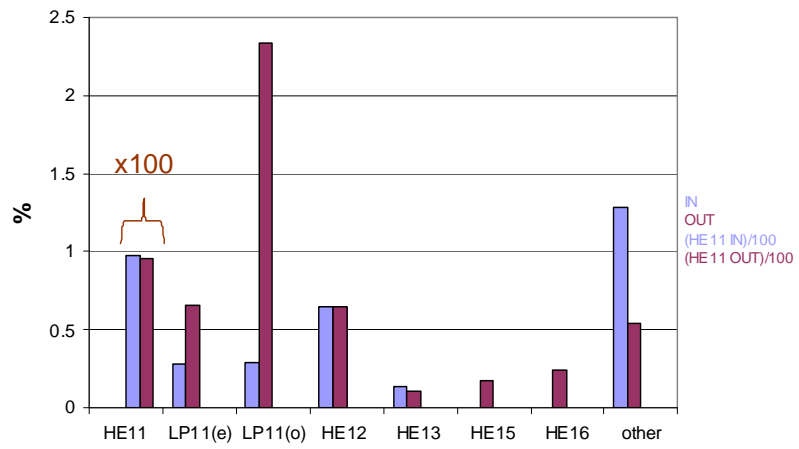


Figure 7. Percentage of modal power in the input and output for the Gaussian beam input that is 97% of HE_{11} mode.

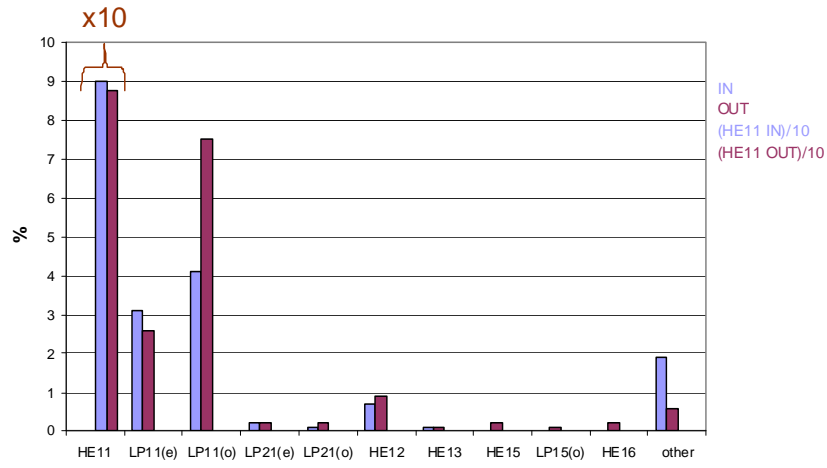


Figure 8. Percentage of modal power in the input and output for the Gaussian beam input that is 90% of HE_{11} mode.

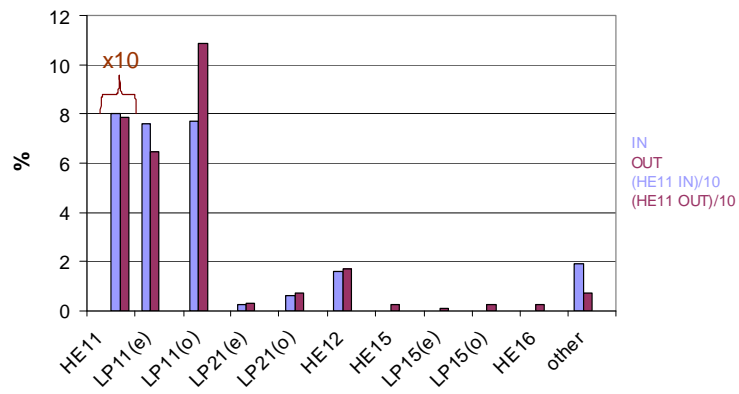


Figure 9. Percentage of modal power in the input and output for the Gaussian beam input that is 80% of HE_{11} mode.

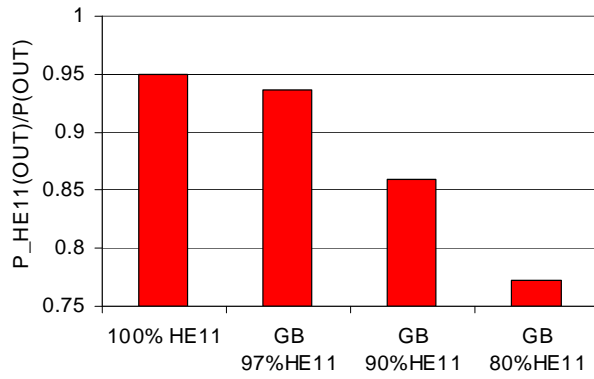


Figure 10. Output HE_{11} mode content: (a) pure HE_{11} mode input; (b)-(d) GB input that is (b) 97% HE_{11} , (c) 90% HE_{11} , (d) 80% HE_{11} .

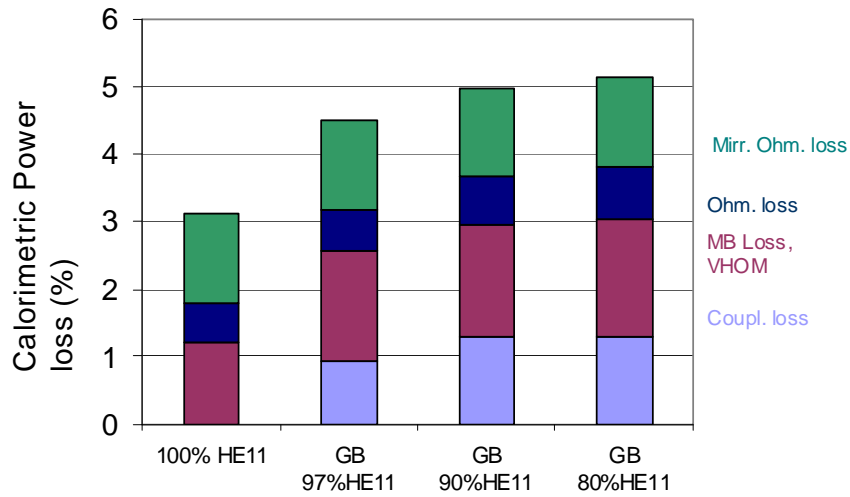


Figure 11. Calorimetric loss (%) in the ITER TL for (a) pure HE₁₁ mode input, (b) Gaussian beam input that is 97% HE₁₁ mode, (c) GB that is 90% HE₁₁, (d) GB that is 80% HE₁₁. Partitions: (1) Coupling losses; (2) Losses in the miter bends due to excitation of very high order modes which add to Ohmic losses; (3) Ohmic losses in straight sections; (4) Ohmic losses in the miter bend mirrors.

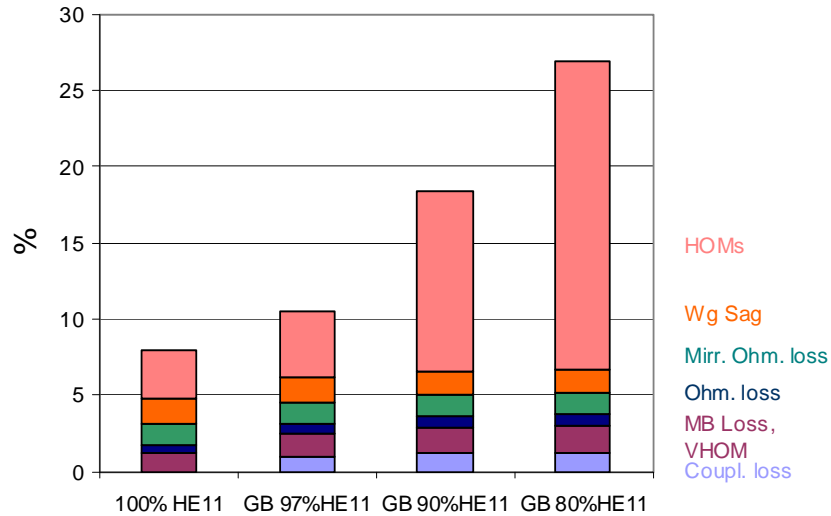


Figure 12. HE₁₁ mode Power Loss (%) in the ITER TL for (a) pure HE₁₁ mode input, (b) Gaussian beam input that is 97% HE₁₁ mode, (c) GB that is 90% HE₁₁, (d) GB that is 80% HE₁₁. Partitions: (1) Coupling losses; (2) Losses in the miter bends due to excitation of very high order modes which add to Ohmic losses; (3) Ohmic losses in straight sections; (4) Ohmic losses in the miter bend mirrors; (5) HE₁₁ mode conversion loss due to sag in waveguide sections and tilt and offset of waveguide section junctions; (6) Losses due to higher order modes in the output beam.

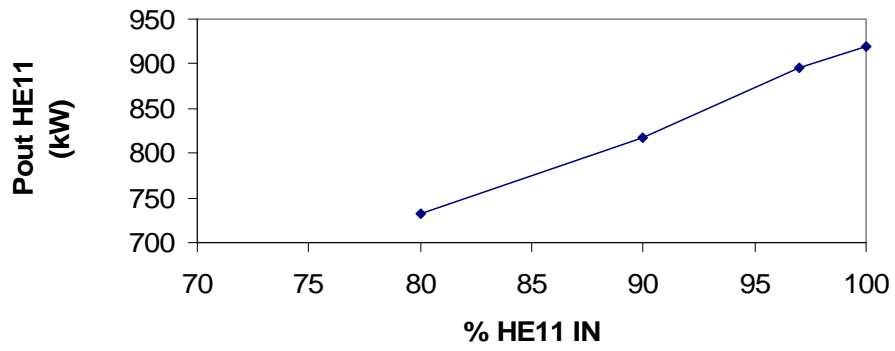


Figure 13. Output power in the HE₁₁ mode versus Percentage of HE₁₁ in the input.